Argon mini-arc meets its match: use of a laser-driven plasma source in ultraviolet-detector calibrations

Uwe Arp,* Robert Vest, Jeanne Houston, and Thomas Lucatorto

Sensor Science Division, National Institute of Standards and Technology,
100 Bureau Dr., Gaithersburg, Maryland 20899, USA

*Corresponding author: uwe.arp@nist.gov

Received 19 December 2013; revised 15 January 2014; accepted 16 January 2014;
posted 22 January 2014 (Doc. ID 203415); published 13 February 2014

The National Institute of Standards and Technology operates two spectral comparator facilities, both of which are used to provide detector calibrations from the ultraviolet to the near-infrared spectral range. One, the Ultraviolet Spectral Comparator Facility (UV SCF), has been in operation for more than two decades, providing one of the core calibration services. Recently, the illumination source used in the UV SCF has been changed from an argon mini-arc source to a laser-driven plasma light source. This new source has higher brightness, a smaller source size, better temporal stability, and much better conversion efficiency than the previous source. The improvements in the capabilities are summarized.

OCIS codes: (040.7190) Ultraviolet; (040.5160) Photodetectors; (120.5630) Radiometry.
http://dx.doi.org/10.1364/AO.53.001089

1. Introduction

Many national measurement institutes, like the National Institute of Standards and Technology (NIST), provide radiometric detector and source calibration services, which span the optical portion of the electromagnetic spectrum. Optical radiation includes the ultraviolet, visible, and infrared spectral regions. NIST operates two spectral comparator facilities, an ultraviolet system, called Ultraviolet Spectral Comparator Facility (UV SCF) [1,2], which covers the wavelength range from 200 to 500 nm, and a visible and near-infrared setup, called Vis/NIR SCF, which covers the wavelength range from 350 to 1800 nm. In both systems, the spectral radiant power responsivity of photodetectors is determined. The absolute spectral power responsivity scale is established using absolute cryogenic radiometers (ACR) [3,4] and transfer standards, usually trap detectors [5] or photodiodes. A cryogenic radiometer uses electrical substitution at liquid-helium temperatures to determine absolute radiant power, i.e., the ACR ties the optical power to the electrical power. Currently, trap detectors and photodiodes are calibrated as transfer standards using tunable lasers and an ACR at the spectral irradiance and radiance responsivity calibrations using uniform sources (SIRCUS) facility [6]. Then working standard detectors are calibrated using the UV SCF and two transfer standard detectors. To accomplish this, a working standard detector is mounted in position P0 (see Fig. 1), and two transfer standard detectors are mounted in positions P1 and P2. In the same way the customer's devices are calibrated using these working standards, working standards are calibrated using transfer standards. For more details on these procedures, see [1].

2. Ultraviolet Spectral Comparator Facility

Figure 1 depicts the UV SCF optical system. The calibrations are performed using the substitution method with monitor, which minimizes uncertainties caused by light source fluctuations. Historically, the light source in the UV SCF was an argon mini-arc source (AMAS) [7,8]. The AMAS was recently replaced by a commercially available laser-driven light source (LDLS) [9,10]. This LDLS is based on a bulb-contained plasma discharge, which is sustained by a continuous near-infrared laser operating at 20 W.

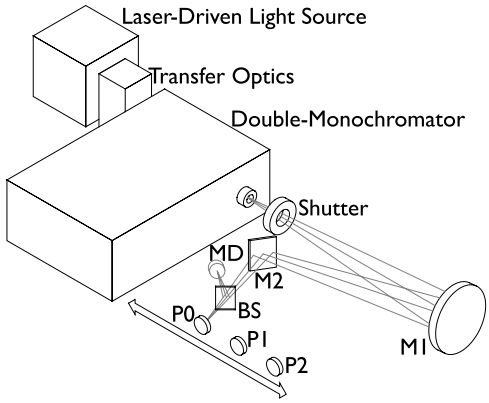

Fig. 1. Schematic layout of the UV SCF. The light generated in the laser-driven light source (LDLS) is imaged onto the entrance slit of the double monochromator using transfer optics. The exit slit of the monochromator is imaged onto the detector under test (P0) or one of two working standard detectors 1 (P1) and 2 (P2), using the spherical mirror M1 and flat mirror M2. Source fluctuations are monitored with a beamsplitter (BS) and monitor detector (MD). The shutter allows measurement of the background signal of the data acquisition system.

The LDLS is coupled into the optical system more efficiently than the AMAS with two off-axis parabolic mirrors (transfer optics in Fig. 1, also Fig. 4). The laser-generated plasma is imaged onto the entrance slit of the double-grating monochromator (double Czerny–Turner configuration), and the exit slit is imaged onto the detector under test or working standard detector, using the spherical mirror M1 and plane mirror M2. Just before the detector plane is a beamsplitter (BS), which reflects a small fraction of the light onto the monitor detector (MD). The shutter shown in Fig. 1 is closed before each measurement to determine the background signal, which is subsequently subtracted from the signal measured with the shutter opened.

In the data-acquisition electronics, the photocurrents generated in the photodiodes are amplified and converted into voltages using transimpedance amplifiers [11]. The photodiodes are operated in the short-circuit arrangement, without a bias voltage. The output voltage of the amplifier is proportional to the photodiode current, as determined by the feedback transimpedance. Currently, the signal from each detector in the UV SCF is amplified with a separate transimpedance amplifier. The gains of these amplifiers were calibrated beforehand and appropriate correction factors applied to the output voltages [12]. These output voltages are read by high-precision digital voltmeters and recorded on a computer.

In the substitution method with monitor, the detector under test (at position P0 in Fig. 1) is calibrated using the following procedure: first the ratio of the signals of the detector under test and the monitor $S_{\mathrm{DUT}}/S_{\mathrm{MD}}$ is measured at each wavelength, e.g., from 200 to 400 nm in 5 nm steps. Then the signal ratios for both working standards, $S_{\mathrm{WSD1}}/S_{\mathrm{MD}}$ and $S_{\mathrm{WSD2}}/S_{\mathrm{MD}}$, are measured. Using these ratios, the known gains of the amplifiers and the spectral power responsivities of the two working standard detectors, the spectral power responsivity of the detector under test can be derived. For more details on the measurement equation and a discussion of the measurement uncertainties, see [1].

3. Laser-Driven Light Source Versus Argon Mini-Arc

In the top panel of Fig. 2, the optical power in the detector plane of the UV SCF for both the argon mini-arc P_{AMAS} and the laser-driven light source P_{LDLS} are shown. Also displayed in the top panel of Fig. 2 is the ratio of the optical power for both sources, $P_{\mathrm{LDLS}}/P_{\mathrm{AMAS}}$. The use of the LDLS in the UV SCF increases the available optical power considerably, especially at wavelengths shorter than 250 nm. The largest optical power increase is at 200 nm, where 12 times more power is available with the LDLS. At wavelengths longer than 250 nm, the available power increased by a factor of about 4.

In the future, we hope to capitalize on this increase in optical power by shortening the calibration chain. Instead of using detectors calibrated in the SIRCUS facility to calibrate working standard detectors in the UV SCF, we are planning to calibrate working standard detectors in the UV SCF directly, using an ACR. This will reduce the uncertainties, especially in the short wavelength range below 250 nm. The

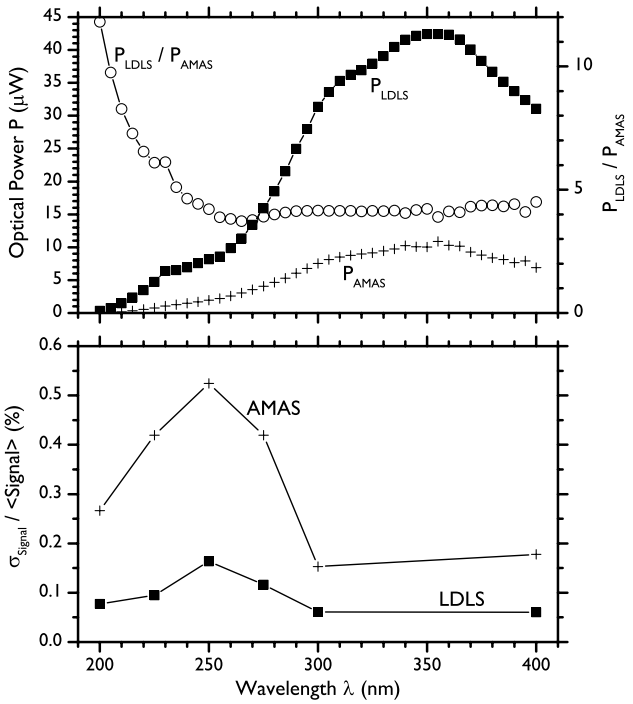

Fig. 2. (Top) Comparison of the optical power at the detector position of the UV SCF: laser-driven light source (LDLS) P_{LDLS} ■, argon mini-arc source (AMAS) P_{AMAS} +. The ratio $P_{\mathrm{LDLS}}/P_{\mathrm{AMAS}}$ is indicated by the open circles ○. (Bottom) Relative standard deviation $\sigma_{\mathrm{Signal}}/\langle\mathrm{Signal}\rangle$ of the detector signal averaged over about 2 min for the LDLS ■ and AMAS +. Decreased stability caused by ozone generation is clearly visible around 250 nm.

ultraviolet lasers used in the SIRCUS facility cannot be tuned to wavelengths shorter than 210 nm. Therefore the calibration of the transfer standard between 200 and 210 nm is based on an extrapolation, which models the data at longer wavelengths. Between 200 and 210 nm, direct calibration of working standard detectors will greatly reduce the uncertainties.

In the bottom panel of Fig. 2, the temporal stability of the two sources is displayed. The relative standard deviation of the mean signal accumulated over about 2 min is shown. The LDLS exhibits better temporal stability by a factor of 2–5. The output of both sources exhibits less stability in the range of the ozone absorption, which peaks around 250 nm [13]. Ozone is produced by both sources through photodissociation of molecular oxygen at wavelengths shorter than about 200 nm [14]. To avoid ozone production in the LDLS, the lamp housing is purged with dry nitrogen. The consequences of the improvement in source stability are shown in Fig. 3. In the top panel of Fig. 3, the difference in data-acquisition statistics using the AMAS and LDLS is displayed. During calibrations in the UV SCF, 10 or more samples are taken at each wavelength, and the mean of these samples is used as the signal ratio value (detector signal/monitor signal). In Fig. 3 the relative standard deviation, $\sigma_{\text{Signal/Monitor}}$, divided by the mean of ⟨Signal/Monitor⟩, is displayed for both sources. The statistics of the data acquisition is improved using the LDLS,

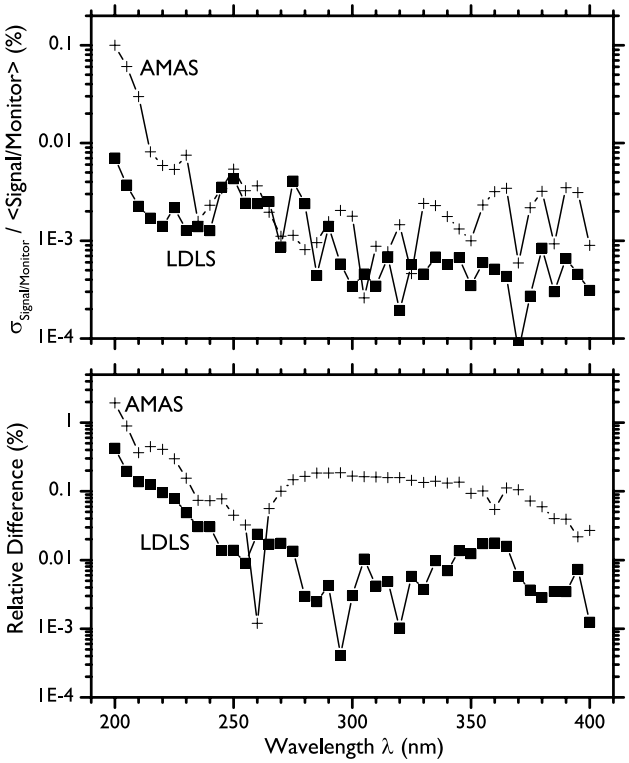

Fig. 3. (Top) Relative standard deviation of 10 samples of the detector signal divided by the monitor signal for the UV SCF in percent: LDLS ■, AMAS +. (Bottom) Difference in results for two measurements of the same detector showing improved repeatability: LDLS ■, AMAS +.

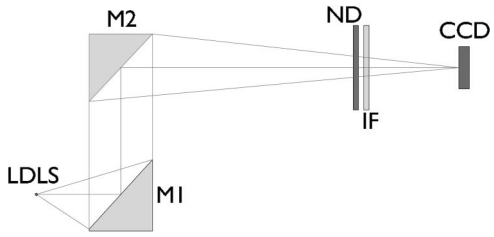

Fig. 4. Schematic layout of the transfer optic, which images the LDLS onto the charged-coupled device camera (CCD), using two off-axis parabolic mirrors. M1 collimates the light, and M2 refocuses the beam onto the CCD. M2 has a four times longer effective focal length than M1, resulting in a four times magnified image and four times reduced divergence of the beam. The neutral density filter (ND) and interference filter (IF) are placed in the beam to reduce the intensity.

again especially at the short-wavelength end. This will reduce the uncertainties of the calibrations provided by the UV SCF.

In the bottom panel of Fig. 3, another indicator of temporal stability is shown. The same photodiode was calibrated twice with each source, and the relative difference in the results is displayed. The repeatability of the measurement using the LDLS is improved, especially at short wavelengths.

To measure the size of the LDLS image after the transfer optics, a CCD camera was placed in the image plane of the pair of off-axis parabolic mirrors. The arrangement is shown in Fig. 4. Because of the high intensity, a neutral density filter, with 0.1% transmission, and an interference filter with a center wavelength of $\lambda_0 = 350$ nm and a bandwidth of $\Delta\lambda = 10$ nm, were placed in front of the CCD camera. The same beam-size measurement system was used in the determination of the electron beam size at the Synchrotron Ultraviolet Radiation Facility SURF III [15] and the source size in deuterium lamps [16]. The camera was used to optimize the image by moving the source relative to the prealigned mirrors (see Fig. 5). A Gaussian fit to the profile results in a vertical FWHM, $\text{FWHM}_y = (602.0 \pm 9.1)$ μm, and

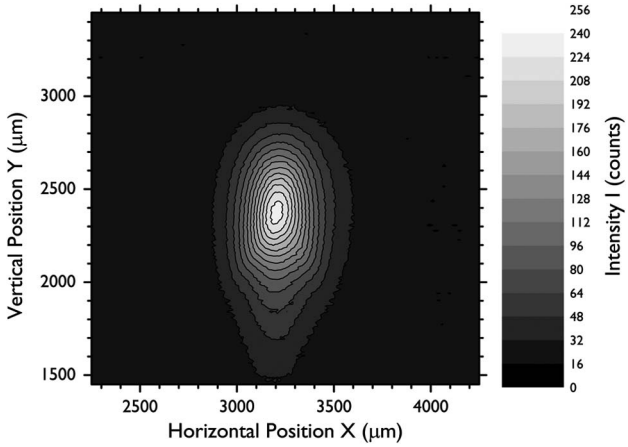

Fig. 5. Image of the LDLS at $\lambda_0 = 350$ in the focus of the transfer optics, which consists of two off-axis parabolic mirrors. The FWHM is (314.8 ± 2.6) μm horizontally and (602.0 ± 9.1) μm vertically.

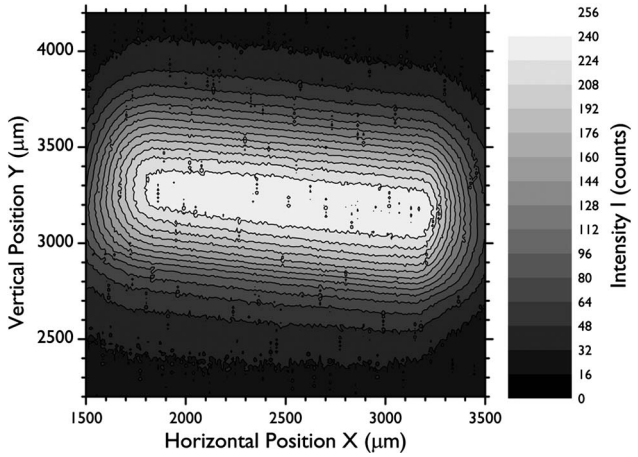

Fig. 6. Image of the UV SCF beam in the detector plane at $\lambda = 400$ nm. The FWHM is (1617.6 ± 60.0) μm horizontally and (720.6 ± 3.9) μm vertically.

horizontal $\text{FWHM}_x = (314.8 \pm 2.6)$ μm, which is considerably smaller than that achievable with the argon mini-arc. The small source size makes the more efficient coupling of the LDLS through the transfer optics, consisting of two off-axis parabolical mirrors, possible. With a larger source size, imaging errors would lead to significant loss of light in the transfer optics. The entrance slit of the monochromator is underfilled by the image of the LDLS.

Also of interest is the size of the beam in the detector plane, especially for irradiance meter calibrations [17], which are based on spatial scanning of detectors through the beam. In Fig. 6, the beam profile in the detector plane is shown. The data were acquired using the same CCD camera as used before to measure the image size after the transfer optics. The monochromator was tuned to 400 nm wavelength for this measurement. The FWHM of the beam in the detector plane is (1617.6 ± 60.0) μm horizontally and (720.6 ± 3.9) μm vertically. The wide horizontal spot size is related to the exit slit size of the monochromator and aberrations caused by spherical mirror M1, which could be reduced by closing the exit slit. This would, however, reduce the bandpass, which is currently $\Delta\lambda \approx 4$ nm, and the optical power. Measurement results at other wavelengths did not differ significantly from the measurement at 400 nm.

There was some concern that the higher optical power will cause detector degradation. However, previous studies [18,19] have shown that silicon-based photodiodes degrade very slowly when exposed to radiation with wavelengths longer than 200 nm. Tests in the UV SCF using the LDLS showed no measurable degradation of a photodiode, which was placed in the detector plane. The studies were performed at $\lambda = 300$, 290, 250, and 225 nm.

4. Conclusion and Outlook

Replacement of the AMAS in the UV SCF by a LDLS significantly increased the available optical power in the detector plane. The boosted optical power will make it possible to shorten the calibration chain, and, in the future, working standard detectors will be calibrated directly against an ACR in the UV SCF, thus eliminating all uncertainties resulting from the use of transfer standards, which were calibrated in a separate system with a different light source and optics. Any uncertainty caused by differences in bandpass, out-off-band radiation, spectral purity, collimation, or data extrapolation will be removed. This will reduce the uncertainties of the calibrations done using the UV SCF, especially in the short-wavelength range below 220 nm.

The LDLS is temporally stabler than the argon mini-arc, which reduces the uncertainties in the data acquisition through improved data-acquisition statistics.

Other benefits of using the LDLS are low power consumption and therefore no increase in ambient temperature, which used to be an issue with the argon mini-arc. In addition, the LDLS is safer to operate than the AMAS because it does not require a high-voltage strike to start the plasma discharge.

The LDLS emits a broadband continuum from the ultraviolet to the near-infrared, making it also useful in the Vis/NIR SCF. First tests were promising and showed significant increase in optical power over the whole spectral range. Using the LDLS in the Vis/NIR SCF will also expand its use to shorter wavelengths, at least down to 300 nm.

The authors would like to thank Drs. Tom Larason, Ping-Shine Shaw, and Eric Shirley for useful discussions during the implementation of this project.

References

1. T. C. Larason and J. M. Houston, "Spectroradiometric detector measurements: ultraviolet, visible, and near-infrared detectors for spectral power," Tech. Rep. SP250-41 (NIST, 2008).
2. T. Larason, S. Bruce, and C. Cromer, "The NIST high accuracy scale for absolute spectral response from 406 nm to 920 nm," J. Res. Natl. Inst. Stand. Technol. **101**, 133–140 (1996).
3. C. R. Yokley, "Long wave infrared testing at NBS," in *Applications of Optical Metrology: Techniques and Measurements II*, J. J. Lee, ed. (SPIE, 1983), Vol. **416**, pp. 2–8.
4. T. J. Quinn and J. E. Martin, "A radiometric determination of the Stefan–Boltzmann constant and thermodynamic temperatures between –40°C and +1100°C," Philos. Trans. Roy. Soc. London A **316**, 85–189 (1985).
5. G. P. Eppeldauer and D. C. Lynch, "Opto-mechanical and electronic design of a tunnel-trap si radiometer," J. Res. Natl. Inst. Stand. Technol. **105**, 813–828 (2000).
6. S. W. Brown, G. P. Eppeldauer, and K. R. Lykke, "Facility for spectral irradiance and radiance responsivity calibrations using uniform sources," Appl. Opt. **45**, 8218–8237 (2006).
7. J. M. Bridges and W. R. Ott, "Vacuum ultraviolet radiometry. 3: the argon mini-arc as a new secondary standard of spectral radiance," Appl. Opt. **16**, 367–376 (1977).
8. J. L. Lean, H. J. Kostkowski, R. D. Saunders, and L. R. Hughey, "Comparison of the NIST SURF and argon miniarc irradiance standards at 214 nm," Appl. Opt. **28**, 3246–3253 (1989).
9. S. Horne, D. Smith, M. Besen, M. Partlow, D. Stolyarov, H. Zhu, and W. Holber, "A novel high-brightness broadband light-source technology from the VUV to the IR," Proc. SPIE **7680**, 76800L (2010).
10. J. Feng, J. Nasiatka, J. Wong, X. Chen, S. E. Hidalgo, T. Vecchione, H. Zhu, F. Javier Palomares, and H. A. Padmore, "A stigmatic ultraviolet-visible monochromator for use with a

high brightness laser driven plasma light source," Rev. Sci. Instrum. **84**, 085114 (2013).
11. G. Eppeldauer and J. E. Hardis, "Fourteen-decade photocurrent measurements with large-area silicon photodiodes at room temperature," Appl. Opt. **30**, 3091–3099 (1991).
12. G. P. Eppeldauer, H. W. Yoon, D. G. Jarrett, and T. C. Larason, "Development of an *in situ* calibration method for current-to-voltage converters for high-accuracy SI-traceable low dc current measurements," Metrologia **50**, 509–517 (2013).
13. E. C. Y. Inn and Y. Tanaka, "Absorption coefficient of ozone in the ultraviolet and visible regions," J. Opt. Soc. Am. **43**, 870 (1953).
14. T. Matsui, A. S.-C. Cheung, K. W.-S. Leung, K. Yoshino, W. H. Parkinson, A. P. Thorne, J. E. Murray, K. Ito, and T. Imajo, "High resolution absorption cross-section measurements of the Schumann–Runge bands of O_2 by VUV Fourier transform spectroscopy," J. Mol. Spectrosc. **219**, 45–57 (2003).
15. U. Arp, "Diffraction and depth-of-field effects in electron beam imaging at SURF III," Nucl. Instrum. Methods Phys. Res. A **462**, 568–575 (2001).
16. U. Arp, R. Klein, Z. Li, W. Paustian, M. Richter, P.-S. Shaw, and R. Thornagel, "Synchrotron radiation-based bilateral intercomparison of ultraviolet source calibrations," Metrologia **48**, 261–267 (2011).
17. P.-S. Shaw, R. Gupta, and K. R. Lykke, "Characterization of an ultraviolet and a vacuum-ultraviolet irradiance meter with synchrotron radiation," Appl. Opt. **41**, 7173–7178 (2002).
18. U. Arp, P.-S. Shaw, R. Gupta, and K. R. Lykke, "Damage to solid-state photodiodes by vacuum ultraviolet radiation," J. Electron Spectrosc. Relat. Phenom. **144–147**, 1039–1042 (2005).
19. R. Gupta, K. Lykke, P. S. Shaw, and J. L. Dehmer, "Characterization of UV-induced Radiation Damage in Si-based Photodiodes," in *Ultraviolet Atmospheric and Space Remote Sensing: Methods and Instrumentation II*, G. R. Carruthers and K. F. Dymond, eds. (SPIE, 1999), Vol. **3818**, pp. 27–33.